Cement and Concrete Research 113 (2018) 169–177

Contents lists available at ScienceDirect

Cement and Concrete Research

journal homepage: www.elsevier.com/locate/cemconres

On the mechanism of prevention of explosive spalling in ultra-high performance concrete with polymer fibers

Dong Zhang[a,b], Aravind Dasari[b,*], Kang Hai Tan[a,*]

[a] School of Civil and Environmental Engineering, Nanyang Technological University, 639798, Singapore
[b] School of Materials Science and Engineering, Nanyang Technological University, 639798, Singapore

ARTICLE INFO

Keywords:
Spalling
Ultra-high performance concrete
Polypropylene fibers
Gas permeability
Thermal mismatch

ABSTRACT

It has been a common practice to use polymer fibers to reduce susceptibility of explosive spalling in ultra-high performance concrete (UHPC). However, to-date, despite the proposition of different mechanisms through which polymer fibers enhance gas permeability and reduce explosive spalling, there are many unanswered questions and unjustified claims on the proposed mechanisms. Therefore, the major emphasis of this work is to thoroughly re-examine and understand the exact role of polymer fibers in the prevention of explosive spalling of UHPC. A range of analytical and microscopic tools are used to realize this objective. It is concluded that melting of polymer fibers and creation of empty channels are not required for enhancing the permeability of gases or water vapor through concrete. In fact, it is the thermal mismatch between embedded fibers and matrix that is critical in obtaining an interconnected network of cracks in the matrix. This occurs even before melting of polypropylene (PP) fibers. The network of cracks is responsible for enhancing permeability, thereby reducing the susceptibility of explosive spalling of UHPC.

1. Introduction

Despite the high compressive strength of ultra-high performance concrete (UHPC) (typically > 150 MPa), it is susceptible to explosive spalling when exposed to fire. As a result of explosive spalling, the rate of heat flow to inner layers of member(s) increases, compromising the load-carrying capacity of structures [1]. The mechanisms for explosive spalling have been studied quite extensively for many decades and it is now widely accepted that a combination of build-up of internal pore pressure and thermal stresses is required for spalling to happen. Simply put, the pore pressure build-up, which is a trigger for spalling, is a result of restricted pathways for evaporated free water and physically-bound water [2,3]. In regions closer to the heated surface, due to restriction of thermal dilatation, compressive (thermal) stresses will develop parallel to the heated surface resulting in spalling [4]. Therefore, thermal characteristics like heating rate play an important role in determining the extent of spalling.

For resisting spalling, different approaches have been proposed to tackle both material-scale phenomena/properties of concrete (improving gas permeability and inherent characteristics like initial moisture content) and structural properties such as steel reinforcement, thickness of concrete cover, etc. [5–7]. As there are many studies on these aspects, to avoid duplication, the authors will only present a critical review of widely-used methodologies of preventing explosive spalling with polymer fibers, which is the focus of this work.

Many spalling prevention mechanisms with PP fibers (added to concrete in the range of 1 to 3 kg/m^3) were proposed, although they have not yet been fully validated by actual spalling test results. These include the formation of pressure-induced tangential space (PITS) [8], interfacial transition zones (ITZ) between the fibers and concrete matrix [9–11], and microcracking at higher temperatures of 200 °C [12] and even at 400 °C [16]. Nonetheless, melting of PP fibers and creation of pathways to relieve the vapor pressure built-up in concrete is the most commonly accepted spalling resistance mechanism in the literature [7,13]. Despite the extensive literature on this topic, many aspects of this proposed mechanism are qualitative, and many questions still remain unanswered. For instance:

(i) what is the role of molten polymer in spalling (which generally happens in the temperature range of 200–300 °C [2])?
(ii) How does this polymer melt flow in concrete so as to create empty channels to release trapped vapor pressure as the polymer does not even start to decompose until 265 °C (onset decomposition temperature, $T_{5\%}$, where 5% of mass loss occurs)?

On this aspect, some studies have claimed that PP melt is partially

* Corresponding authors.
E-mail addresses: aravind@ntu.edu.sg (A. Dasari), CKHTAN@ntu.edu.sg (K.H. Tan).

https://doi.org/10.1016/j.cemconres.2018.08.012
Received 10 October 2017; Received in revised form 4 June 2018; Accepted 31 August 2018
Available online 08 September 2018
0008-8846/

Table 1
Mixture compositions of UHPC (unit in kg/m^3).

W/B[a]	Cement[b]	Silica fume	Silica sand	Superplasticizer	Fine aggregate	Water	PP fiber[c]
0.2	830	208	208	33	913	208	3

[a] W/B: water to binder ratio.
[b] Portland cement (ASIA@CEM II 52.5 R).
[c] PP fiber was added only in UHPC/F.

absorbed by cement matrix [14,15]. However, it is difficult to accept this considering the high melt viscosity (600–1000 Pa·s at 250 °C depending on applied shear rate) and size (hydrodynamic volume) of the polymer chains. Another important aspect is the significant increase in permeability of UHPC including high-performance concrete (HPC) even below the melting temperature of PP fibers [16–18]. For example, Bošnjak et al. [18] noted that the permeability of concrete with PP fibers shows a sudden increase of approximately two orders of magnitude (from $\sim 3 \times 10^{-18}$ m^2 to 2×10^{-16} m^2) between 80 °C and 130 °C. In this regard, the major focus of this work is to thoroughly re-examine the exact role of PP fibers in the prevention of explosive spalling of UHPC. For this purpose, a range of analytical, physical and microscopic characterization techniques are used on the concrete samples before and after subjecting to elevated temperature.

2. Experimental work

2.1. Materials and sample preparation

The mix proportion of materials used for UHPC in this study is shown in Table 1. The mean size of silica sand was 110 μm. Natural river sand with the maximum size of 0.6 mm was used as fine aggregate. PP fibers with a density of 910 kg/m^3 and an aspect ratio of ~360 (12 mm length and 33 μm diameter) were obtained commercially. Polycarboxylic type superplasticizer (Sika ViscoCrete-2044) was used in all concrete mixtures. Samples of UHPC with and without PP fibers, were denoted as UHPC/F and UHPC/O, respectively, hereafter. The specimens were demolded after casting for 1 day and stored in lime-saturated water at ambient temperature for 27 days. The compressive strength values of UHPC with and without PP fibers at 28 days were ~148.6 ± 3.0 MPa and 159.9 ± 2.9 MPa, respectively.

The samples for permeability test were cast in disc-shaped molds with 45 mm depth and 150 mm in diameter. After curing, the discs were grinded on both faces and smoothened, with a final thickness of ~40 mm. Cylinder-shaped samples with 50 mm diameter and 100 mm height were also prepared for spalling tests at elevated temperature.

2.2. Thermal analysis

Differential scanning calorimeter (DSC, from TA Instruments, model: Q10) and thermogravimetric analysis (TGA, from TA Instruments, model: Q500) were conducted to understand the melting and decomposition behavior of PP fibers and concrete mix. A constant heating rate of 5 °C/min from room temperature to 400 °C was employed in DSC, while in TGA, a ramp of 5 °C/min was used to heat up to 400 °C in the air atmosphere. The gas flow used in both DSC and TGA was set at 100 ml/min. To understand the dimensional changes and variations in coefficient of thermal expansion (CTE) of fibers, cement paste and aggregates with temperature, thermomechanical analyzer (TMA, from TA Instruments, model: Q400) was employed. The samples were heated in a furnace with a probe in contact that is connected to a strain detector and a force generator. The force was set at 0.01 N. For the cement paste and aggregate, the samples were heated to 300 °C with a heating rate of 5 °C/min, while the maximum temperature of 150 °C was used for PP fibers. All the TMA tests were performed under nitrogen atmosphere.

2.3. X-ray diffraction

X-ray diffraction (XRD) measurements using CuKα radiation were conducted on UHPC/O and UHPC/F to identify the crystal phases. The sample sections were 18 mm in length, 12 mm in width and 3 mm in thickness. Four batches of samples were prepared for each mix for testing at different selected temperatures, i.e., ambient, 105 °C, 150 °C and 250 °C. Since spalling of concrete usually occurs at a temperature ranging from 200 °C to 300 °C [2,19], only behaviors under 300 °C are of interest in this study.

2.4. Microscopic observations and crack quantification

A scanning electron microscope (SEM, JSM 6360) operating at an accelerating voltage of 5 kV was used for observing microstructural changes of UHPC/F and UHPC/O at different temperatures after carefully preparing the samples following a series of grinding and polishing steps. 800, 1200 and 2500 grit sandpapers were used for initial grinding of the samples for 0.5 min, 2 min and 10 min, respectively. Then, the samples were polished on a Buehler TexMet P cloth (hard perforated and non-woven) by using 1 μm diamond paste for 20 min. Afterwards, the samples were rinsed for 5 min with isopropanol in an ultrasonic bath. For each target temperature (chosen as 105 °C, 150 °C, 170 °C, 200 °C and 300 °C), to obtain information before and after melting of fibers, samples were kept in a convection furnace for approximately 30 min. Subsequently, they were allowed to cool down naturally in the furnace.

To observe a representative area/number of fibers at high resolution (for identifying microcracks in samples) in an SEM micrograph, 25 micrographs at a fixed magnification (500×, covering an area of 256 × 192 μm^2) were taken and stitched together. This selection was based on the findings in [26,27] where it was noted that 20 frames of images at a magnification of 500× were necessary for meaningful image analysis. To perform an accurate fully-automated image analysis for quantification of microcracks, it is a requirement that the original image is of exceptional resolution with good contrast and have sharp transitions from white to black (and vice versa). Generally, SEM micrographs of concrete do not possess these qualities, and therefore, automated detection and crack segmentation methods are usually unreliable. Hence, a semi-automated approach was adopted here. The stitched SEM micrograph was converted to a binary image in which the pixels of microcracks were set to 1 (black) and the pixels of background were defined as 0 (white) by using Fuji/ImageJ software, developed by National Institutes of Health (NIH) [20]. This was followed by manual tracing using Photoshop. Finally, image analysis was performed. Based on isotropy hypothesis of crack distribution and statistics for crack length, stereology parameters were extracted from 2D images to describe the networks of cracks [21–23]. In this study, number density of microcracks (total number of microcracks divided by the image area), crack area fraction (% of crack area to the image area) and crack connectivity were quantified. Crack network (connectivity), ϕ, is defined by the following equation [22]:

$$\varnothing = 1 - \sum_{j=1}^{m} l_j^2 / \sum_{k=1}^{n} l_k^2$$

where m and n represent the number of isolated and total number of

microcracks, respectively. l_j is the respective length of the j^{th} isolated microcrack and l_k is the respective length of the k^{th} microcrack.

2.5. Gas permeability measurements

Both residual and hot permeability values of UHPC/O and UHPC/F were measured. In residual permeability test, samples were heated by using an electrical furnace with a heating rate of 1 °C/min to all the selected temperatures, followed by maintaining at the target temperature until a constant mass (equilibrium) was reached to exclude the effect of moisture. Afterwards, samples were naturally cooled down to about 60 °C in the furnace. Subsequently, samples were sealed in a desiccator containing silica gel and naturally cooled down to room temperature. After each heat treatment, residual permeability of the specimen was measured using Torrent permeability tester, which was a standard handheld permeability device developed by Torrent [24] and was further analyzed for general applications by Jacobs and Hunkeler [25]. Three specimens of each concrete mix were employed in the test and the average values were reported here. Additionally, hot permeability of UHPC/O and UHPC/F samples were also measured at the same target temperature. At least two specimens of each concrete mix were tested. Details of the test setup and procedure for evaluating hot permeability are given in [16].

2.6. Spalling tests

Spalling tests were conducted to show the effectiveness of PP fibers in preventing spalling of UHPC. Three cylinders with 50 mm diameter and 100 mm height were tested for each mix. The cylinders were heated in an electrical furnace for 1 h in accordance with the standard ISO 834 heating curve. Afterwards, the cylinders were allowed to cool down naturally in the furnace for 24 h. Then the extent of spalling was measured and documented.

A summary of the tests conducted in this investigation is shown in Table 2.

3. Result and discussion

3.1. Spalling behavior and the extent of gas permeability

As evident in Fig. 1, the presence of PP fibers in UHPC mitigated explosive spalling when exposed to ISO 834 heating curve. However, the samples without PP fibers exhibited severe spalling with the entire specimen breaking into small pieces. As a first step to explain these differences, both residual and hot permeability values of UHPC with and without fibers are shown in Fig. 2 as a function of temperature. Due to the dense microstructure of UHPC, it was difficult to obtain gas permeability of UHPC at ambient temperature. Therefore, UHPC was dried at 105 °C before measuring the permeability, in line with other reported studies [16,21]. In general, the gas permeability increased with increasing temperature for both UHPC/O and UHPC/F. Also, in the presence of fibers, at any measured temperature, residual permeability of UHPC/F was always larger than UHPC/O. More importantly, permeability of UHPC/F showed a significant increase by two-orders of magnitude between 105 °C and 150 °C. The permeability further increased by one-order of magnitude between 150 and 200 °C. With a further increase in temperature beyond 200 °C, the rate of increase in gas permeability of UHPC/F is less. Furthermore, it should be noted that despite the quantitative differences between residual and hot permeability data, both follow a very similar trend. The quantitative differences are expected as there are fundamental variations between residual and hot permeability techniques. For example, residual permeability values are based on air viscosity, whereas hot permeability values are dependent on vapor viscosity, and their respective mobility through the network of cracks in the concrete sample. There are other facets that could influence the differences in quantitative data obtained from these two techniques like the closure of cracks during cooling down, recrystallization/solidification of PP, and the differences in testing methodologies by themselves. However, to what extent these different factors are contributing to the differences between hot and residual permeability is beyond the scope of this study, and the authors will investigate this aspect in detail in their future work. In the current work, the intention is to show that a similar trend of permeability (especially, the increase in permeability of UHPC/F at 150 °C) is observed irrespective of the technique.

Table 2
Summary of tests.

Sample	Tests
Concrete (UHPC/F and UHPC/O)	Residual permeability Hot permeability Spalling test DSC, TGA, XRD, SEM
PP fiber	TGA, DSC
Cement paste, aggregate, PP	TMA

The permeability results of UHPC/F (Fig. 2) are extremely interesting as a significant increase of two-orders of magnitude was observed even before reaching the melting point of PP fibers (which is ~170 °C) (Fig. 3). This clearly suggests the failure of many theories that have been proposed to account for the improvement in spalling resistance of UHPC with PP fibers. It is also evident from Fig. 3 that the decomposition onset of PP fibers is well beyond 250 °C, and at 350 °C the mass loss is almost 97%, which again illustrates the failure of 'melting of PP fibers and creation of empty channels' theory for relieving the vapor pressure developed in the concrete. Further, XRD spectra of UHPC/O and UHPC/F subjected to different temperatures are similar qualitatively (in terms of peak positions) with no obvious differences (Fig. 4). This clearly indicates the absence of any chemical/phase changes in UHPC until 250 °C.

Findings from XRD data are also supported by the DSC and TGA data of UHPC/O and UHPC/F (Fig. 5), which suggest the absence of phase changes of UHPC until 250 °C. As evident, below 200 °C, there are only peaks related to evaporation of free water. Subsequently, at around 250 °C, dehydration of calcium silicate hydrate (C-S-H) phase causes the loss of bond water [26]. In short, XRD and DSC-TGA data of UHPC/O and UHPC/F suggest that the changes in permeability cannot be attributed to any of the phase/chemical changes of concrete.

3.2. Dimensional changes with temperature

As explained in Section 3.1, considering the size (12 mm in length and 33 μm diameter) and number density of PP fibers in the concrete matrix ($3.2 \times 10^8/m^3$), the significant increase in permeability between 100 °C and 150 °C cannot be explained by any of the mechanisms proposed in the literature. The authors believe that melting of fibers is not related at all to the observed increase in permeability of concrete matrix. The differences in coefficient of thermal expansion or in other words mismatch of thermal expansion between the polymer and the concrete is the key parameter. To explain this further, dimensional changes with increase in temperature of cement paste, aggregate and PP fibers are shown in Fig. 6. Clearly, PP fibers show relatively much larger dimensional changes than cement paste when exposed to high temperature. At 105 °C, the relative dimensional change of PP fibers is almost 41 times larger than that of cement paste, and it further increases at 150 °C. This provides the first clue of what exactly happens even before melting of fibers. The huge difference in CTE of PP and cement paste is capable of resulting in the formation of microcracks at the interface of PP fibers. This relieves the build-up of internal stresses through the formation of a permeable transport system for escaping water vapor (permeation effect) if the number density of fibers is high enough to create an interconnected network of cracks.

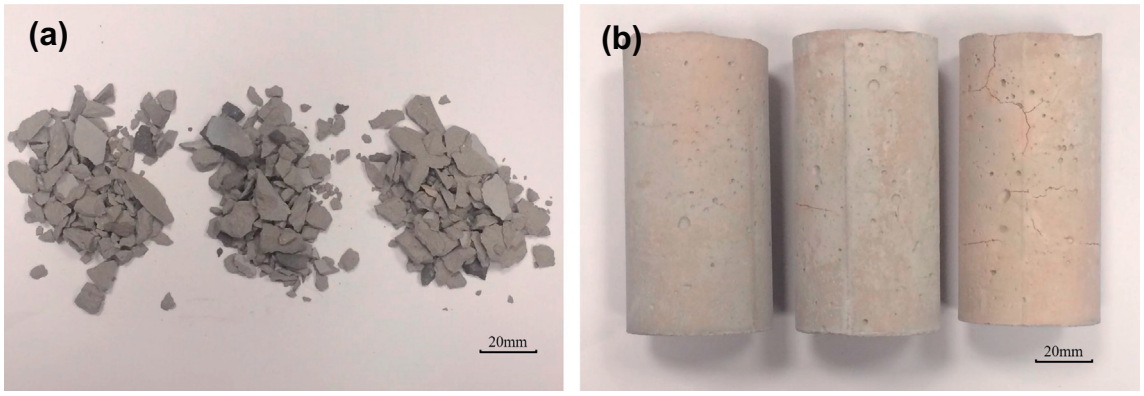

Fig. 1. Results of spalling test for (a) UHPC without fibers, and (b) UHPC with fibers subjected to standard ISO 834 heating curve for 1 h.

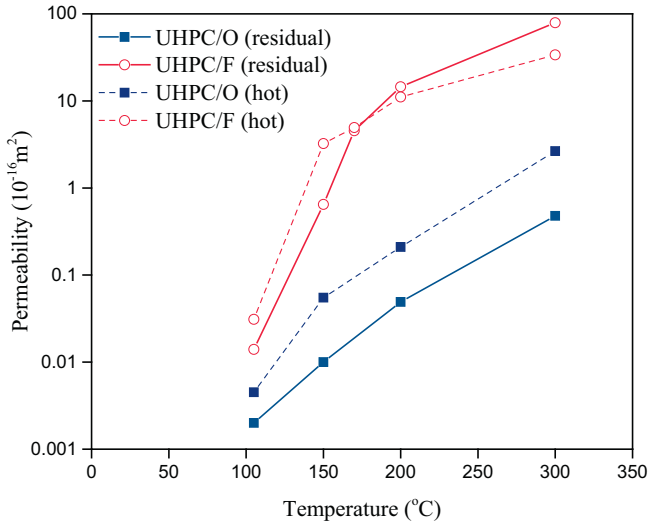

Fig. 2. Residual and hot gas permeability of UHPC with and without fibers and with increasing temperature.

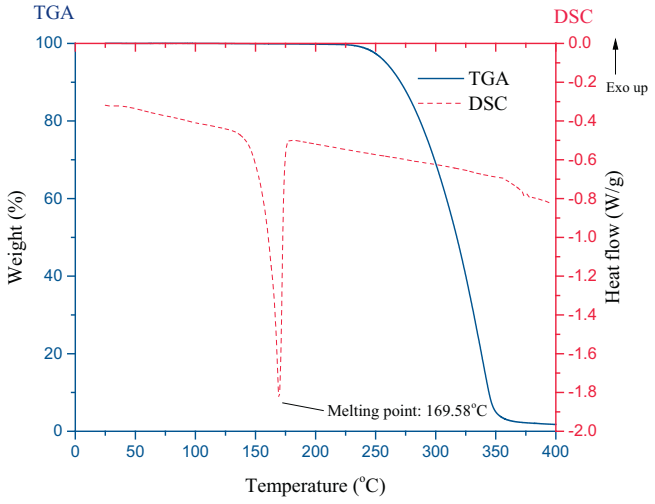

Fig. 3. TGA-DSC data of PP fibers used in the current study.

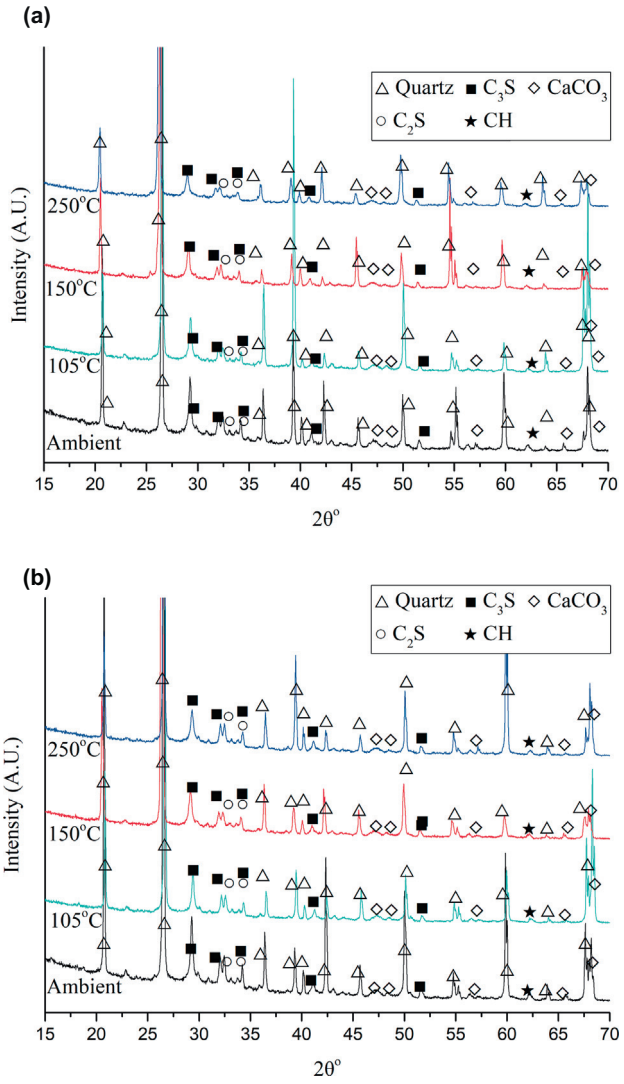

Fig. 4. XRD spectra of (a) UHPC/O and (b) UHPC/F subjected to different temperatures. C_2S is dicalcium silicate, C_3S tricalcium silicate, and CH calcium hydroxide.

In fact, the phenomenon of mismatch of CTEs is widely reported in the composites field (for example, see [27]). The mismatch between the CTE of the matrix and the fibers could result in stresses (during cooling from high temperatures) that are often sufficient to produce micro-cracking even in the absence of external loads. Cracks are reported to develop at the interface of fibers and matrix at 45° and then advance into the matrix until they reach adjacent fibers. The relative dimensional changes between cement paste and aggregates at higher temperatures (> 160 °C and up to 300 °C) could also result in microcracks originating at the interface of aggregates. Therefore, it is expected that

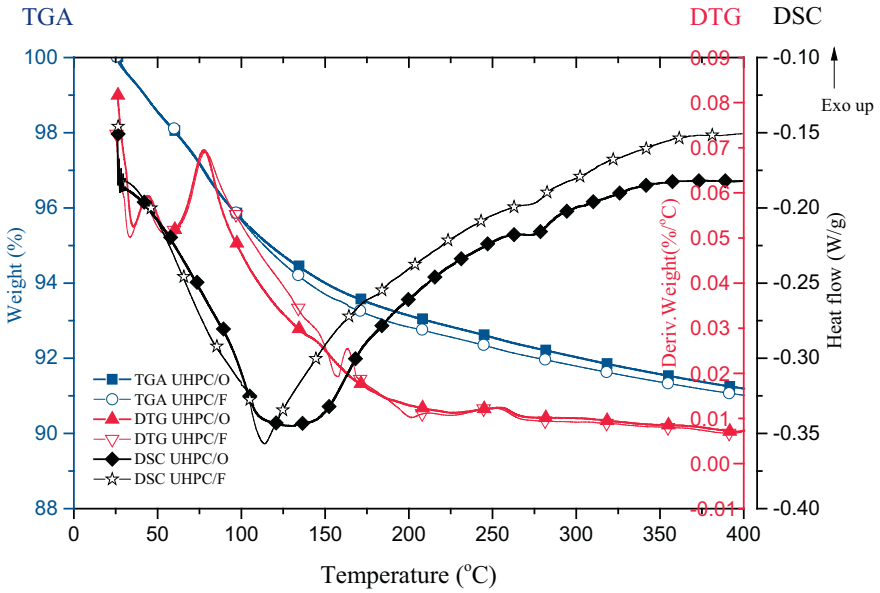

Fig. 5. TGA and DSC data of UHPC/O and UHPC/F.

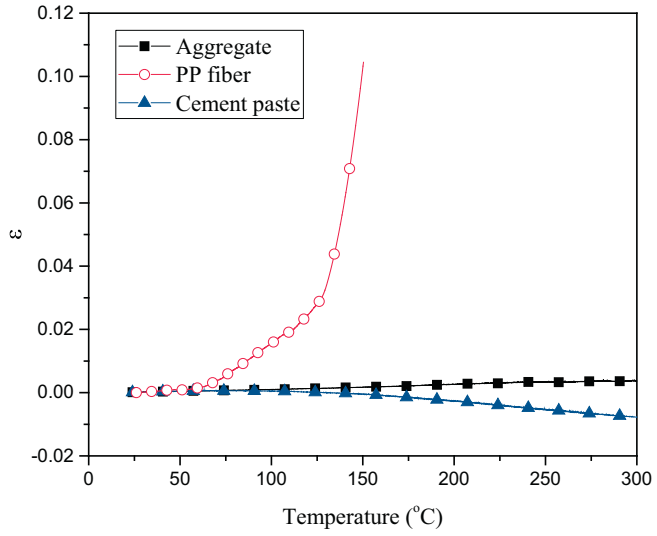

Fig. 6. Dimensional (strain) changes of PP, cement paste and aggregates with temperature. As can be seen, the dimensions of PP increased significantly with temperature. Based on these experiments, CTE of PP is 1.367×10^{-4}/°C below 80 °C, 3.896×10^{-3}/°C between 80 °C and 105 °C, and 2.084×10^{-3}/°C between 105 °C and 150 °C.

even the aggregate size and volume fraction will influence the formation of microcracks induced by aggregate restrained shrinkage (due to differences in expansion/shrinkage coefficient mismatch between aggregate and concrete). However, considering the aspect ratio of the aggregate in the present system (~1.2), the contribution of this to the overall network of microcracks is expected to be small.

3.3. Microscopic investigation of the role of PP fibers

To understand the microstructural evolution in UHPC/F with changes in temperature, a representative area was chosen containing a few fibers and exposed to different temperatures. An SEM micrograph of this representative region at different temperatures is shown in Fig. 7. At ambient temperature, there are no obvious cracks around the fibers and fine aggregates (0.6 mm) (Fig. 7a). After exposing the sample to 105 °C, some microcracks appear around the PP fibers, as shown in Fig. 7b. This is a result of mismatch in expansion coefficients of PP fibers and matrix or in other words, caused by restrained expansion of PP fibers. According to Fig. 6, the dimension change of PP fibers at 105 °C in unconstrained conditions is already 41 times than that of cement paste. Though the fibers are not completely debonded, Fig. 7b clearly reveals that the formation of microcracks starts at the interface in the radial direction.

If loading were to be applied on these samples along with a rising temperature, then there may be further widening of microcracks or even closing depending on the type of imposed loading. Here, temperature is the only variable and changes in microstructure (and thus, permeability) can be directly related to it. At 150 °C, the size and length of cracks increase along with the appearance of new radial cracks from fibers to matrix. These microcracks are found to link those created by the neighboring fibers and form an interconnecting network, as shown in Fig. 7c. Moreover, the inset in Fig. 7c shows a higher magnification SEM micrograph of the PP fiber interface. It clearly points to debonding of fibers from the matrix. This reiterates that thermal stresses caused by the mismatch in thermal expansion coefficients of the fibers and matrix phases are large enough to cause microcracking of the matrix.

Similar microcracks are also observed as a result of aggregate restrained shrinkage in [21,28]. Lu et al. [29] have characterized the matrix cracking in brittle matrix composites induced by mismatch of thermal expansion coefficients between the matrix and the fiber by using a non-dimensional cracking coefficient. The magnitude of this coefficient was governed by incompatible strain, matrix toughness and modulus, fiber size and volume fraction. In these matrices, it was noted that interfacial debonding encouraged matrix cracking and that the cracks extended radially between the fibers. In the current test specimens, as the PP fiber has a higher CTE than the matrix, the matrix is in compression and should in fact provide resistance to matrix crack opening. However, the occurrence of debonding at the interface and matrix cracking suggests that the relative difference in CTE is too large. Besides, the cement paste shrinks at higher temperatures.

Therefore, it can be concluded that the network of cracks formed throughout the matrix initiated from the fiber-matrix interface is the primary reason for the huge increase in gas permeability at temperatures < 170 °C. This is also evident from the calculations of crack density, crack connectivity and crack area fraction in the samples (Fig. 9), which show an increase from 105 °C to 150 °C and 170 °C. The crack connectivity, in particular, is an important (geometrical) factor

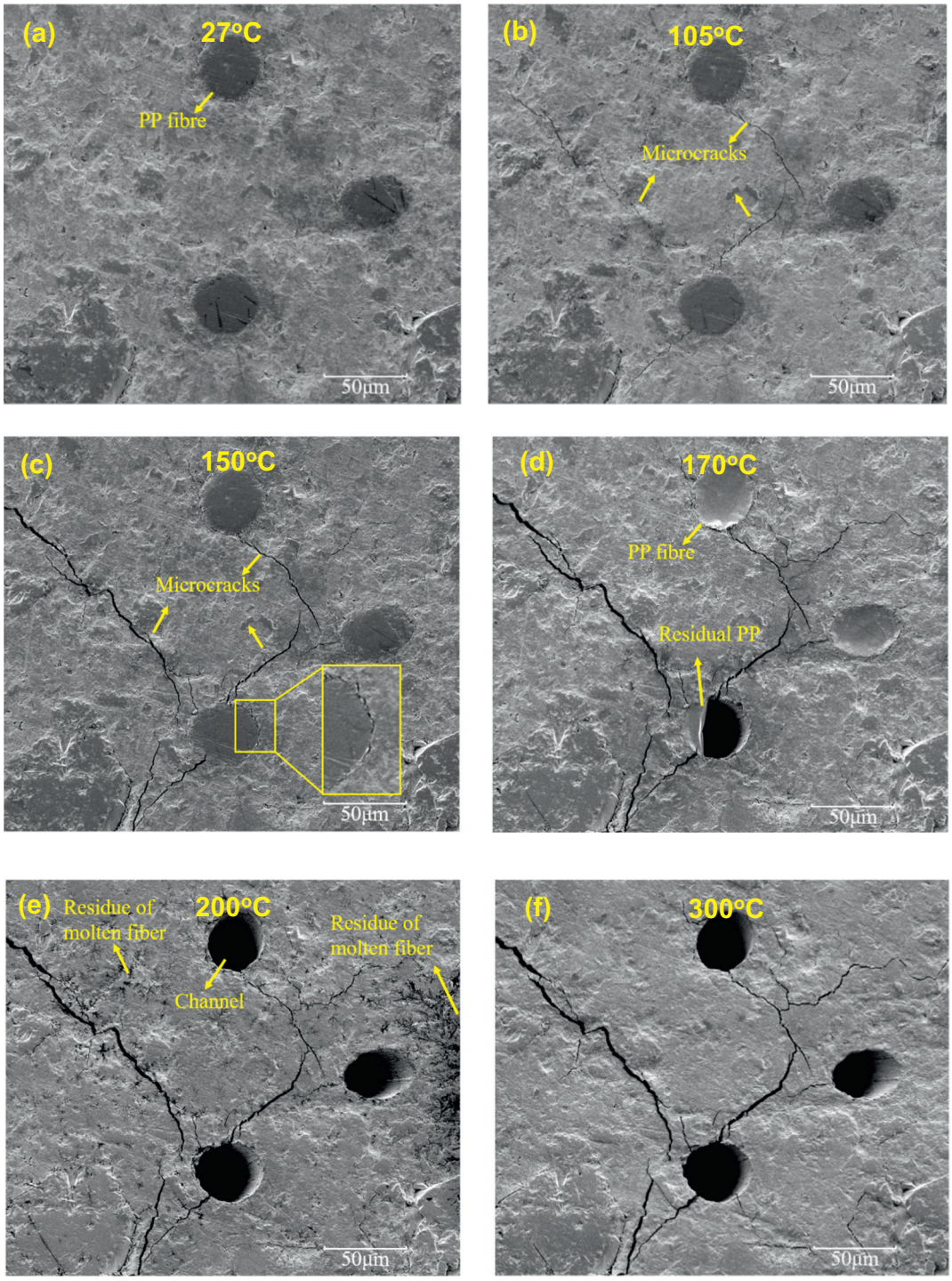

Fig. 7. Microstructural evolution in UHPC/F sample with temperature: (a) ambient temperature; (b) 105 °C; (c) 150 °C; (d) 170 °C; (e) 200 °C; and (f) 300 °C.

governing gas permeability through concrete [30]. At 170 °C, which is the peak of the melting endotherm of PP fiber, some PP fibers disappeared partially from their channels (Fig. 7d). Nevertheless, new microcracks have been observed at 170 °C, and more importantly, the existing microcracks widened and grew in length and in width. As the onset decomposition of PP fibers is around 265 °C, this suggests that the molten polymer might have flown into surrounding cracks. However, absorption of melt by surrounding matrix is not possible due to the highly viscous nature of the melt. In fact, the authors have carried out a simple experiment on this aspect where a few PP fibers were sandwiched between a glass slide and UHPC. The setup was heated to 200 °C and maintained at that temperature for 1 h. After cooling down from heating, cross-sections at different places were cut and checked for the absorption of melted PP fibers into concrete. Little evidence of melted PP penetrating into UHPC was found.

At higher temperatures of 200 °C and 300 °C (Fig. 7e and f), most of the PP fibers have disappeared. Importantly, the disappearance of fibers and the creation of empty channels did not contribute significantly to the permeability of concrete at these temperatures (Fig. 2). This is despite an increase in the total crack area fraction due to the empty channels left behind by PP fibers (Fig. 8c). This reiterates the importance of creation of interconnected network of cracks at

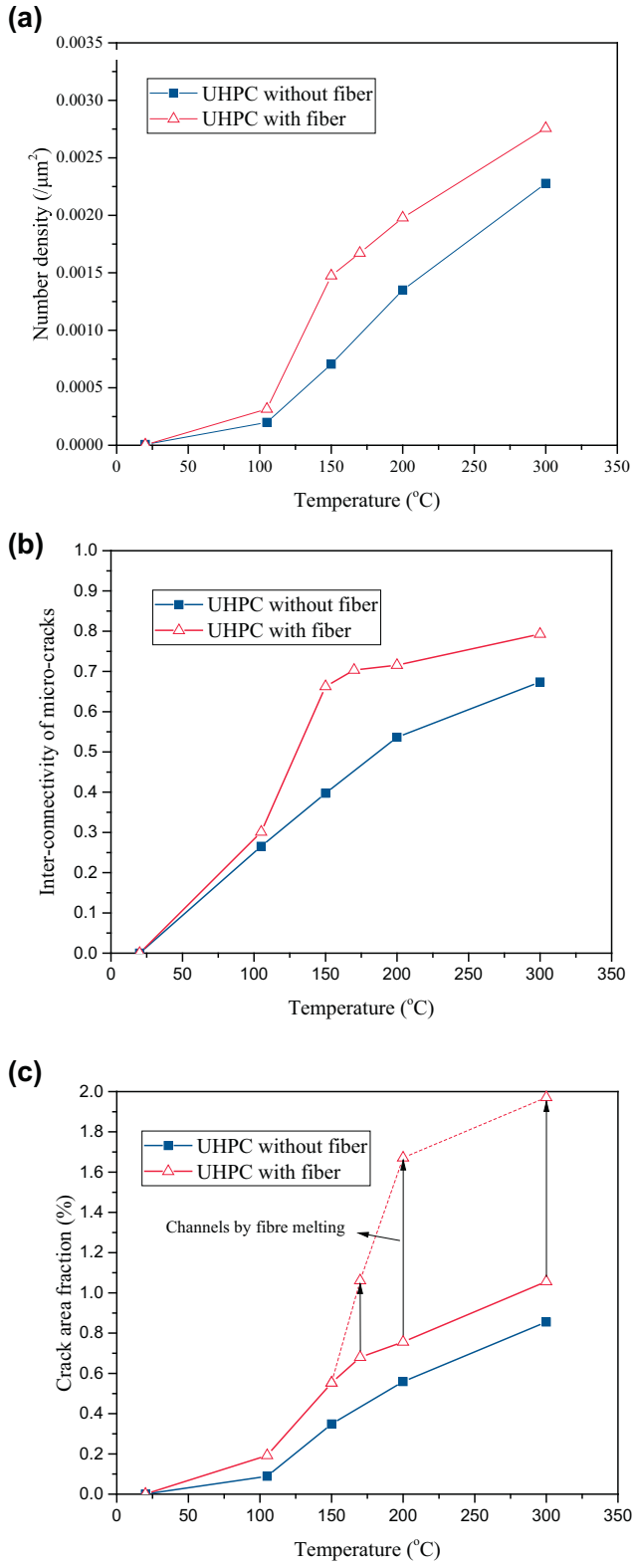

Fig. 8. Changes in (a) number density, (b) inter-connectivity, and (c) area fraction of microcracks with temperature. Dotted line in (c) considered the areas left by melted fibers.

temperatures lower than the melting point of fibers.

In contrast, in the absence of fibers, the number of microcracks formed in UHPC sample is small even at a high temperature of 200 °C. An example of this behavior is shown in Fig. 9, which clearly indicates the absence of interconnected network of cracks. This is expected considering the size and number density of aggregates, as well as the relatively small thermal mismatch between aggregates and cement paste (Fig. 6). This ultimately resulted in limited number of microcracks extending from the interface of aggregates into concrete matrix. Essentially, the permeability of UHPC/O at temperature of 200 °C remained at a relatively lower level.

Nonetheless, it must be highlighted that the crack network in these samples is expected to be of three-dimensional, and thus, the increase in inter-connectivity (Fig. 8b) is even more significant. The observations presented in Figs. 7 and 9 and the associated crack calculations in Fig. 8 are based on two-dimensional analysis only. A further investigation by using 3D X-ray tomography would be excellent to support the important findings. But the required high resolution of tomography versus the size of sample may compromise the scale of observations, as the recommended sample size is 1000 to 2000 times of the resolution in X-ray tomography [31]. To achieve a submicron resolution, the sample size should be < 1 mm.

In summary, this work sheds light on the mechanism of prevention of explosive spalling in concrete with polymer fibers. The results presented here show that the proposed mechanism of melting of polymer fibers in enhancing the permeability of gases through concrete may not be a correct reflection of the actual behavior observed. The thermal mismatch between the fibers and the matrix is critical for obtaining an interconnected network of cracks in the matrix even before melting of fibers. In fact, these observations suggest that polymer fibers per se are not required and even other choice of materials may be able to increase the permeability of concrete. The requirements for the materials are: (i) exhibit a huge thermal mismatch with the cement matrix, and (ii) high aspect ratio of the fibers. The higher the aspect ratio of the fibers, the greater the number density of these dispersed particles in the matrix, the higher will be the crack density and interconnectivity. More importantly, this work provides the foundation and solutions for resisting explosive spalling in concrete with compressive strength of > 150 MPa. This means by simply focusing on the phase boundary between the polymer fibers and the matrix, it is possible to tackle spalling by initiating a network of fine cracks upon an increase in temperature.

4. Conclusions

This study re-examines the mechanism of preventing spalling of UHPC by polymer fibers. Based on the experimental results, it is confirmed that polymer fibers improve the spalling resistance of UHPC by increasing the gas permeability with temperature. The permeability of UHPC showed two-order increase in magnitude when exposed to 150 °C, which is below the melting point of PP fibers. The permeability further increased by another order of magnitude between 150 and 200 °C. With a further increase in temperature (to 200 °C and even 300 °C), the rate of increase in gas permeability in the presence of fibers is relatively small. This suggests that the empty channels (of PP fibers) left behind do not contribute significantly to the permeability of concrete. This reiterated the importance of the creation of interconnected network of cracks at temperatures lower than the melting point of fibers. The formation of microcracks is a result of huge mismatch in thermal expansion coefficients of the matrix and the fibers. This is confirmed by TMA and supported by SEM observations. Further, XRD and TGA-DSC results of concrete with and without fibers also confirmed the absence of any chemical/phase changes of UHPC at temperatures < 250 °C, which is the critical range for permeability measurements.

Acknowledgements

This research/work is supported by the Singapore Ministry of National Development and National Research Foundation under L2 NIC, Award No. L2NICCFP1-2013-4. The authors would like to thank Professor Chen Tsuhan for his valuable suggestions on crack

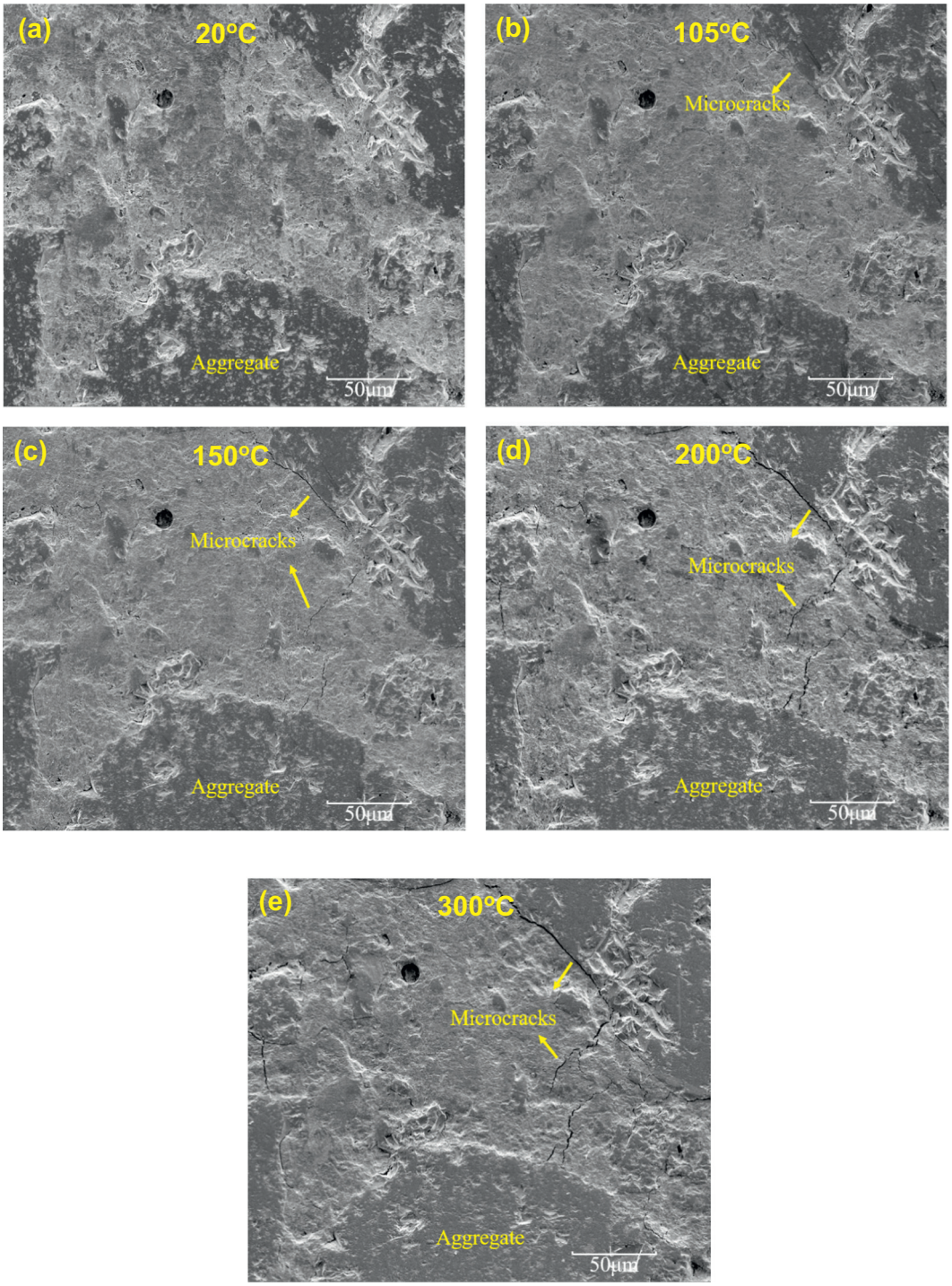

Fig. 9. Microstructural evolution in UHPC/O sample with temperature: (a) ambient temperature; (b) 105 °C; (c) 150 °C; (d) 200 °C; and (e) 300 °C.

measurement. The authors also would like to thank Professor George L England from Imperial College London for his valuable suggestions.

Disclaimer

Any opinions, findings, and conclusions or recommendations expressed in here are those of the author(s) and do not necessarily reflect the views of the MND-NRF.

References

[1] V.K.R. Kodur, L. Phan, Critical factors governing the fire performance of high strength concrete systems, Fire Saf. J. 42 (2007) 482–488.
[2] G.A. Khoury, Effect of fire on concrete and concrete structures, Prog. Struct. Eng. Mater. 2 (2000) 429–447.
[3] J.-C. Liu, K.H. Tan, D. Zhang, Multi-response optimization of post-fire performance of strain hardening cementitious composite, Cem. Concr. Compos. 80 (2017) 80–90.
[4] Z.P. Bažant, Analysis of pore pressure, thermal stress and fracture in rapidly heated concrete, Proceedings of the International Workshop on Fire Performance of High-strength Concrete, National Institute of Standards and Technology (NIST), Gaithesburg, USA, 1997, pp. 155–164.
[5] J.-C. Liu, K.H. Tan, Fire resistance of strain hardening cementitious composite with hybrid PVA and steel fibers, Constr. Build. Mater. 135 (2017) 600–611.

[6] Y.-S. Heo, J.G. Sanjayan, C.-G. Han, M.-C. Han, Relationship between inter-aggregate spacing and the optimum fiber length for spalling protection of concrete in fire, Cem. Concr. Res. 42 (2012) 549–557.
[7] M.B. Dwaikat, V.K.R. Kodur, Fire induced spalling in high strength concrete beams, Fire. Technol 46 (2010) 251–274.
[8] G.A. Khoury, Polypropylene fibres in heated concrete. Part 2: pressure relief mechanisms and modelling criteria, Mag. Concr. Res. 60 (2008) 189–204.
[9] D.P. Bentz, Fibers, percolation, and spalling of high-performance concrete, ACI Mater. J. 97 (2000) 351–359.
[10] G. Mazzucco, C.E. Majorana, V.A. Salomoni, Numerical simulation of polypropylene fibres in concrete materials under fire conditions, Comput. Struct. 154 (2015) 17–28.
[11] M. Zeiml, D. Leithner, R. Lackner, H.A. Mang, How do polypropylene fibers improve the spalling behavior of in-situ concrete? Cem. Concr. Res. 36 (2006) 929–942.
[12] K. Pistol, F. Weise, B. Meng, U. Schneider, E. Koenders, F. Dehn, The mode of action of polypropylene fibres in high performance concrete at high temperatures, Proceedings of the 2nd International RILEM Workshop on Concrete Spalling Due to Fire Exposure, Delft, The Netherlands, 2011, pp. 5–7.
[13] M. Ozawa, H. Morimoto, Effects of various fibres on high-temperature spalling in high-performance concrete, Constr. Build. Mater. 71 (2014) 83–92.
[14] P. Kalifa, G. Chene, C. Galle, High-temperature behaviour of HPC with polypropylene fibres: from spalling to microstructure, Cem. Concr. Res. 31 (2001) 1487–1499.
[15] R. Jansson, Fire Spalling of Concrete: Theoretical and Experimental Studies, KTH Royal Institute of Technology in Stockholm, Sweden, 2013.
[16] Y. Li, K.H. Tan, M.E.M. Garlock, V.K.R. Kodur (Eds.), Effects of polypropylene and steel fibers on permeability of ultra-high performance concrete at hot state, Structures in Fire (Proceedings of the Ninth International Conference), DEStech Publications, Princeton University, 2016, pp. 145–152.
[17] I. Hager, T. Tracz, The impact of the amount and length of fibrillated polypropylene fibres on the properties of HPC exposed to high temperature, Arch. Civ. Eng. 56 (2010) 57–68.
[18] J. Bošnjak, J. Ožbolt, R. Hahn, Permeability measurement on high strength concrete without and with polypropylene fibers at elevated temperatures using a new test setup, Cem. Concr. Res. 53 (2013) 104–111.
[19] E.W.H. Klingsch, Explosive Spalling of Concrete in Fire, Institute of Structural Engineering, Swiss Federal Institute of Technology in Zurich (ETHZ), 2014.
[20] M.D. Abràmoff, P.J. Magalhães, S.J. Ram, Image processing with ImageJ, Biophoton. Int. 11 (2004) 36–42.
[21] Z. Wu, H.S. Wong, N.R. Buenfeld, Influence of drying-induced microcracking and related size effects on mass transport properties of concrete, Cem. Concr. Res. 68 (2015) 35–48.
[22] C. Zhou, K. Li, X. Pang, Geometry of crack network and its impact on transport properties of concrete, Cem. Concr. Res. 42 (2012) 1261–1272.
[23] H.-L. Wang, J.-G. Dai, X.-Y. Sun, X.-L. Zhang, Characteristics of concrete cracks and their influence on chloride penetration, Constr. Build. Mater. 107 (2016) 216–225.
[24] R.J. Torrent, A two-chamber vacuum cell for measuring the coefficient of permeability to air of the concrete cover on site, Mater. Struct. 25 (1992) 358–365.
[25] F. Jacobs, F. Hunkeler, Non destructive testing of the concrete cover–evaluation of permeability test data, in: I.d.C.d.M.d. Madrid (Ed.), International RILEM Workshop on Performance Based Evaluation and Indicators for Concrete Durability, RILEM Publications, Madrid, Spain, 2006.
[26] A. Noumowe, Mechanical properties and microstructure of high strength concrete containing polypropylene fibres exposed to temperatures up to 200 °C, Cem. Concr. Res. 35 (2005) 2192–2198.
[27] E.S. Folias, M. Hohn, Predicting crack initiation in composite material systems due to a thermal expansion mismatch, Int. J. Fract. 93 (1998) 335–349.
[28] P. Grassl, H.S. Wong, N.R. Buenfeld, Influence of aggregate size and volume fraction on shrinkage induced micro-cracking of concrete and mortar, Cem. Concr. Res. 40 (2010) 85–93.
[29] T.C. Lu, A.G. Evans, R.J. Hecht, R. Mehrabian, Toughening of $MoSi_2$ with a ductile (niobium) reinforcement, Acta Metall. Mater. 39 (1991) 1853–1862.
[30] E. Ringot, A. Bascoul, About the analysis of microcracking in concrete, Cem. Concr. Compos. 23 (2001) 261–266.
[31] N. Bossa, P. Chaurand, J. Vicente, D. Borschneck, C. Levard, O. Aguerre-Chariol, J. Rose, Micro- and nano-X-ray computed-tomography: a step forward in the characterization of the pore network of a leached cement paste, Cem. Concr. Res. 67 (2015) 138–147.